Noname manuscript No.
(will be inserted by the editor)

Influence of Westerly Wind Events stochasticity on El Niño amplitude: the case of 2014 vs. 2015.

Puy Martin · Jérôme Vialard · Matthieu Lengaigne · Eric Guilyardi · Pedro N. Di Nezio · Aurore Voldoire · Magdalena Balmaseda · Gurvan Madec · Christophe Menkes · Michael J.Mcphaden

Received: date / Accepted: date

Abstract The weak El Niño of 2014 was preceded by anomalously high equatorial Pacific Warm Water Volume (WWV) and strong Westerly Wind Events (WWEs), which typically lead to record breaking El Nino, like in 1997 and 2015. Here, we use the CNRM-CM5 coupled model to investigate the causes for the stalled El Niño in 2014 and the necessary conditions for extreme El Niños. This model is ideally suited to study this problem because it simulates all the processes thought to be critical for the onset and development of El Niño. It captures El Niño preconditioning by WWV, the WWEs characteristics and their deterministic behaviour in response to warm pool displacements. Our main finding is, that despite their deterministic control, WWEs display a sufficiently strong stochastic component to explain the distinct evolutions of El Niño in 2014 and 2015. A 100-member ensemble simulation initialized with early-spring equatorial conditions analogous to those observed in 2014 and 2015 demonstrates that early-year elevated WWV and strong WWEs preclude the occurrence of a La Niña but lead to El Niños that span the weak (with few WWEs) to extreme (with many WWEs) range. Sensitivity experiments confirm that numerous/strong WWEs shift the El Niño distribution toward larger amplitudes, with a particular emphasis on summer/fall WWEs occurrence which result in a five-fold increase of the odds for an extreme El Niño. A long simulation further demonstrates that sustained WWEs throughout the year and anomalously high WWV are necessary conditions for extreme El Niño to develop. In contrast, we find no systematic influence of easterly wind events (EWEs) on the El Niño amplitude in our model. Our results demonstrate that the weak amplitude of El Niño in 2014 can be explained by WWEs stochastic variations without invoking EWEs or remote influences from outside the tropical Pacific and therefore its peak amplitude was inherently unpredictable at long lead-time.

Keywords El Niño · Westerly wind events · Easterly wind events · Predictability · extreme El Niño events · El Niño predictors

M. PUY
LOCEAN-IPSL Paris, France
E-mail: martin.puy@locean-ipsl.upmc.fr

1 Introduction

The El Niño Southern Oscillation (ENSO) is the most prominent year-to-year climate fluctuation on earth (McPhaden et al, 2006a). El Niño, the positive phase of ENSO, is characterized by an equatorial Pacific anomalous warming peaking near the end of the calendar year, and occurs every 2 to 7 years. On some occasions, these El Niño events can be exceptionally large, as in 1982, 1997 and 2015, with surface temperature (SST) anomalies in the equatorial eastern Pacific exceeding 2.5°C (Fig. 1a). These extreme events result in a massive reorganization of tropical atmospheric convection (Cai et al, 2014) and have particularly strong impacts on extreme weather events such as cyclones, marine and terrestrial ecosystems and agriculture worldwide (McPhaden et al, 2006a).

El Niño grows as a result of the Bjerknes feedback (Bjerknes, 1966), a positive feedback loop between the ocean and atmosphere in the equatorial Pacific. An initial warm SST anomaly in the central Pacific, usually during boreal spring, drives enhanced deep atmospheric convection and westerly wind anomalies. This in turn induces eastward currents and deepens the thermocline in the central/eastern equatorial Pacific, reinforcing the initial warming. The onset of an El Niño event tends to be favored when the equatorial upper Pacific ocean is anomalously warm (Jin, 1997). The Warm Water Volume (WWV), defined as the anomalous volume of water warmer than 20°C in the equatorial Pacific (Meinen and McPhaden, 2000, Fig. 1a,b), is for instance a widely used El Niño predictor, with a 0.6 lead-correlation six months before the peak of El Niño (McPhaden, 2015).

Atmospheric high frequency forcing can also promote the development and/or initiation of El Niño events (e.g. McPhaden and Yu, 1999; Boulanger et al, 2001, 2004; Vecchi and Harrison, 2000; Lengaigne et al, 2004a; Seiki and Takayabu, 2007a; Fedorov et al, 2015; Larson and Kirtman, 2015) by affecting the equatorial SSTs , amplified afterward by the Bjerknes feedback. In the equatorial Pacific, this high frequency atmospheric forcing mostly occurs under the form of synoptic short-lived westerly wind events (WWEs), characterized by westerly wind anomalies lasting between 5 and 30 days, with typical amplitudes of 5 m.s-1 and zonal and meridional extent of 30° and 10° respectively (Harrison and Vecchi, 1997; Seiki and Takayabu, 2007a,b; Puy et al, 2015). They preferentially occur over the western Pacific warm pool during boreal winter and spring and are effective triggers for El Niño when the WWV is anomalously high (Ludescher et al, 2014; Lengaigne et al, 2002; Vitart et al, 2003). WWEs are an essential contributor to El Niño diversity, in terms of timing (Jin et al, 2007), magnitude (Eisenman et al, 2005) and spatial pattern (Lian et al, 2014).

WWEs were initially thought to be purely stochastic, occurring randomly and independently from ENSO (Penland and Sardeshmukh, 1995; Kessler et al, 1995; Kleeman and Moore, 1997), hence raising concerns for El Niño predictability (Fedorov et al, 2003). There is now a clear body of evidence (Eisenman et al, 2005; Gebbie et al, 2007; Gebbie and Tziperman, 2009a; Seiki and Takayabu, 2007a; Puy et al, 2015) that WWEs occur more frequently when the western Pacific warm pool is abnormally shifted to the east. For instance, a very strong WWE in March 1997 (e.g. McPhaden and Yu, 1999; Yu and Rienecker, 1999; Boulanger et al, 2001, 2004) shifted the warm pool eastward via anomalous zonal advection (Lengaigne et al, 2004a). This promoted an eastward expansion of the deep atmospheric convection, favouring the occurrence of subsequent WWEs later in

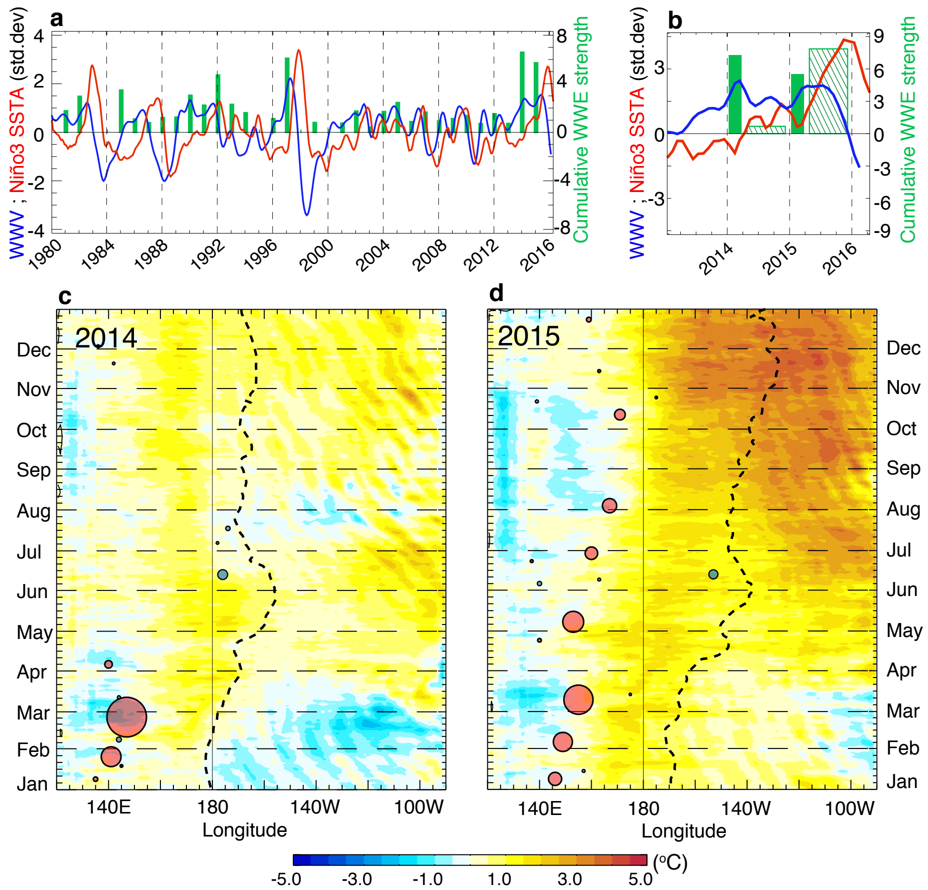

Fig. 1 a, b, Time evolution of (red) standardized Niño3 SSTA (std.dev=1.24°C, see methods) and (blue) WWV anomalies from (a) 1981 to present (5-month running mean) and (b) from 2013 to early 2016 (monthly values). The green bars on panels a and b display the cumulative Westerly Wind Events (WWEs) strength (a good proxy of their oceanic dynamical response, see methods) for the January-March period. c, d, 2014 and 2015 time-longitude section of averaged 2°N-2°S SST anomalies, and WWEs (red circles) and EWEs (easterly wind events, blue circles). The size of the circles that indicate the wind events central dates and longitudes is proportional to the wind event strength. The black line indicates the eastern edge of the western Pacific warm pool (i.e the 28.5 isotherm).

the year (Lengaigne et al, 2004b), and the development of the extreme 1997/98 El Niño. This positive loop between the large-scale SST field (i.e. the warm pool eastward extension) and WWEs numbers and magnitude (Eisenman et al, 2005; Gebbie et al, 2007; Lengaigne et al, 2003; Puy et al, 2015) can be viewed as an intraseasonal component of the Bjerknes feedback. Studies indicating that WWEs are modulated by the large scale SST field raised hopes for the potential to improve ENSO prediction (Gebbie and Tziperman, 2009a,b; Lopez and Kirtman, 2014). Yet, the occurrence of individual WWEs cannot be predicted more than a couple of weeks ahead because they are not only influenced by large-scale conditions but also by shorter time-scale atmospheric processes (Seiki and Takayabu, 2007a; Puy et al, 2015). In addition, while WWEs are more likely to occur when the warm pool is shifted eastward, there is still a stochastic component in their number, amplitude or location that limits ENSO predictability.

The stark contrast in the evolution of the Pacific in 2014 and 2015 is a compelling reminder of the competing role of the deterministic vs. stochastic WWEs behaviour on El Niño evolution and predictability. Operational forecasts in spring 2014 predicted the advent of an El Niño at the end of the year. (Ludescher et al, 2014; Tollefson, 2014; McPhaden, 2015). The WWV index reached the highest value since 1997 during January to March of 2014 (Fig. 1ab). This period also witnessed the strongest series of WWEs since 1997 (Menkes et al, 2014, Fig. 1ab). These early WWEs shifted the warm pool towards the central Pacific (160°W in May 2014, Fig. 1c, Menkes et al, 2014), laying the ground for subsequent WWEs. The ensemble-mean of the European Centre for Medium-Range Weather Forecasts (ECMWF) seasonal forecasts (Molteni et al, 2011) initialized on the 1st of April 2014 predicted a moderate El Niño (Fig. 2a). Early 2015 was very similar to early 2014 in terms of positive WWV anomaly and early-year WWE activity (Fig. 1b). The April 2015 ECMWF forecasts were also similar to those of 2014 and their ensemble mean again pointing to a moderate (but slightly stronger) El Niño (Fig. 2b). The resemblance between these forecasts likely arose from the similar upper heat content and WWEs precursors. Yet, 2014 developed into an at most weak "borderline" El Niño (McPhaden, 2015), while 2015 ranked amongst the strongest El Niños on record, comparable in strength to those of 1997 and 1982 (Fig. 1a).

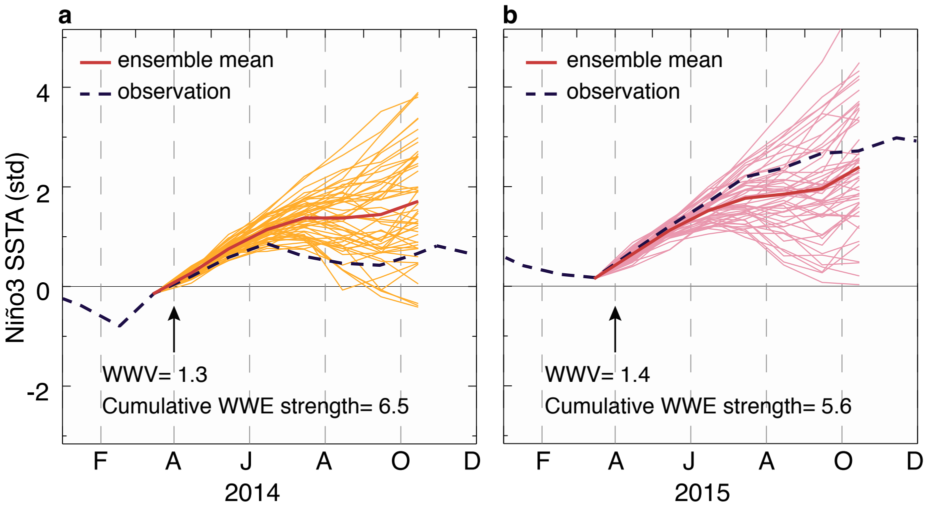

Fig. 2 a, b, Standardized Niño-3 SST anomaly plume from ECMWF 51-members ensemble forecasts initialized on the 1st April 2014 and 2015. The dashed line on panels a, b represents the 2014-2015 observed Niño-3 SST anomaly and the red line on panels a,b,c the ensemble mean.

What caused the different evolution of the El Nino events of 2014 and 2015? Several authors argued that high-frequency wind variability in summer 2014 could be responsible for the failure of El Niño (Hu and Fedorov, 2016; Menkes et al, 2014). The occurrence of Easterly wind events (EWEs, Fig. 1c) , the eastward counterpart to WWEs (Chiodi and Harrison, 2015; Puy et al, 2015), possibly in relation with extra-tropical forcing (Min et al, 2015), could have halted the development of El Niño in 2014 (Hu and Fedorov, 2016). On the other hand, the lack of summer WWEs could also explain why no El Niño developed in 2014 (Menkes et al, 2014). Although the warm pool was shifted eastward, increasing the probability of occurrence of subsequent WWEs, there was no enhanced WWE activity after the early-year WWEs in 2014 as compared to 2015 (Fig. 1b). Using coupled model ensemble experiments initialized with SSTs only in early 2014 and 2015, Larson and Kirtman (2015) also suggested that these two events falls well within the expected uncertainty for noise-driven error growth independent from ENSO. While some external factors may have contributed to suppress WWEs activity in summer 2014 (McPhaden, 2015; Hu and Fedorov, 2016; Levine and McPhaden, 2016; Zhu et al, 2016; Min et al, 2015), this could also have happened by random chance (i.e. due to the stochastic part of the WWEs).

Understanding why two similar early-year conditions led to such different outcomes is an important question, as extreme El Niños such as in 1982/83, 1997/98 or 2014/15 have impacts that are disproportionately stronger relative to weaker El Niños (Cai et al, 2014). Yet, the mechanisms giving rise to extreme El Niño events are still debated (Barnston et al, 2012). In this study, we investigate whether WWEs stochasticity can yield either a 2014-like weak El Niño or a 2015-like extreme El Niño when the initial state is similar to that in early 2014 and 2015. To reach that goal, we use dedicated numerical simulations using a coupled general circulation model that simulates reasonably well El Niño events, WWEs and their mutual relationship. The datasets and model set up are presented in section 2. The good performances of the model are described in section 3. In section 4, we show that conditions similar to those observed in 2014 and 2015 can lead to either a weak or extreme El Niño, depending on the spring and fall WWE activity, while EWEs play a less systematic role. In section 5, we further show that both a recharged WWV and strong summer-fall WWEs are necessary conditions to yield an extreme El Niño. We also use sensitivity experiments to demonstrate that, even in presence of a recharged WWV, the lack of WWEs can increase by up to 5 the odds of a weak 2014-like El Niño, compared to when WWEs occur. A summary and a discussion about these findings are finally provided in section 6.

2 Data and methods

2.1 Climate indices and datasets

We use TropFlux (Kumar et al, 2013) daily zonal wind stresses (http://www.incois.gov.in/tropflux/), weekly sea level anomaly from AVISO (http://www.aviso.oceanobs.com/en/data/products/) and SST from the NOAA optimum Interpolation dataset (Reynolds et al, 2002). Anomalies with respect to the long-term mean seasonal cycle (over 1980-2015 except for sea-level: 1992-2015), are simply referred to as anomalies. The observed WWV index, defined as the anomalous volume of Pacific waters above the 20°C isotherm averaged within the equatorial band (5°N-5°S, 120°E-80°W) (Meinen and McPhaden, 2000), is derived from temperatures analyses based on in situ data (https://www.pmel.noaa.gov/elnino/upper-ocean-heat-content-and-enso). ENSO evolution is characterized as the 3-month running mean of SST anomalies in the Niño3 region (5°N-5°S; 150°W-90°W). The Warm pool eastern edge (WPEE), a measurement of the eastward expansion of the warm pool, is computed as the location of the 28.5°C isotherm in the same dataset. WWV and Niño3 indices are normalized by their standard deviation and have no units. El Niño events are classified into three amplitude categories, based on the value of the standardized December Niño3 SST anomaly: "Neutral state" events for a value below 1.25, "Moderate" El Niños for a value between 1.25 and 2.5 and "extreme" El Niños for a value exceeding 2.5. With this definition, 2014, which is considered as a borderline (i.e. weak) El Niño (McPhaden, 2015) according to some criteria, falls in the "Neutral state" category while 1982, 1997 and 2015 fall into the "extreme" El Niño category.

The oceanic dynamical response to WWEs depends on the intensity, duration and zonal fetch of the intraseasonal wind stress forcing. The "WWE strength", defined as the space-time integration of the zonal wind stress intraseasonal anomalies over the wind event patch and normalized by its standard deviation, computed over all the detected WWEs, is then a good proxy of the WWE-induced oceanic impact ("WEI" in Puy et al (2015)). We define the "early-year" and "subsequent" strength as the cumulative wind event strength for January to March and April to November, respectively, as a way to characterize the impact of episodic wind forcing on the ocean during these periods. Since this cumulative value is based on normalized values, it has no units.

To investigate the role of WWEs in El Niño predictability, sensitivity experiments where WWEs are removed during the model computation (more details about these experiments in section 2.3.1) are performed. Such experiments would be, however, extremely difficult to conduct with Puy et al (2015)'s WWEs definition, which allows to properly compute the "WWE strength", because it requires to have the zonal wind stress field 45 days before and after a given WWE in order to compute the intraseasonal anomalies needed for the detection. Fortunately, WWEs stand out from the seasonal and interannual variability (Equatorial intraseasonnal zonal wind stress average standard deviation of 0.026 N.m-2 between 120°E and the dateline compared to 0.01 N.m-2 for the interannual and seasonal variability). Therefore, defining the WWEs as 2°N-2°S averaged zonal wind stress that exceed 0.025 N.m-2 (corresponding to one standard deviation of the 2°N-2°S average wind stress in the western-central Pacific) during at least 5 days with a 10° minimum zonal extension, gives similar results compared to Puy et al (2015) in term of WWEs "strength" (0.98 correlation between the WWEs detected using the present method and Puy et al (2015)'s method). Because this method doesn't require anomalies to detect the WWEs, it's simpler to implement in a numerical modelling strategy (more details about these experiments in section 2.3.1).

EWEs have however a weaker amplitude than WWEs, comparable to seasonal and interannual wind stress variations (Puy et al, 2015). The method described above for the WWEs is then not relevant regarding EWEs detection. Furthermore, no sensitivity experiment has been performed where the EWEs are removed. We hence keep Puy et al (2015) method and define the EWEs as 2°N-2°S averaged zonal wind stress intraseasonal anomalies (5 to 90 days bandpass filtered using a triangle filter) that exceed -0.04 N.m-2 during at least 5 days with a 10° minimum zonal extension.

2.2 ECMWF ensemble forecasts

We also use ECMWF ensemble seasonal forecasts (Molteni et al, 1996) of Niño3 SST anomalies starting on the 1st of April 2014 and 2015. The forecasts are initialized using ocean and atmosphere observations. The ocean initial conditions are key for ENSO prediction; they are produced through the data assimilation of temperature and salinity in situ profiles, as well as sea level anomalies from satellite altimeter and sea surface temperature (Balmaseda et al, 2013). This information is evolved in time via a coupled ocean-atmosphere circulation model, whose components are to a large extent similar to those in the CNRM-CM5 coupled model, used in the present study. An ensemble of 51 members is produced in order to take into account uncertainty in initial conditions and model formulation (Weisheimer et al, 2014): the spread in error forecast is hence essentially due to the amplification of initial and model errors by the ocean-atmosphere chaotic behaviour. The forecast anomalies are then obtained from the difference to the model climatology (Stockdale et al, 1998).

2.3 CNRM-CM5 model

2.3.1 Model and reference experiment description

The numerical simulations in this study are performed with the earth system model CNRM-CM5 (Voldoire et al, 2013), used in the Fifth Coupled Model Intercomparison Project. Its oceanic component, NEMO v3.2 (Nucleus for European Modelling of the Ocean") is a primitive equation ocean general circulation model, with a free sea surface (Roullet and Madec, 2000). It has a 1° nominal resolution with a meridional refinement of 1/3° at the equator (i.e. ORCA1 configuration, Hewitt et al, 2011). The model has 42 vertical levels, with a resolution ranging from 10m near the surface to 300m at 5000m. The vertical mixing parametrization uses a Turbulent Kinetic Energy (TKE) closure model based on a prognostic vertical turbulent kinetic equation (Blanke and Delecluse, 1993). The lateral mixing is applied using a Laplacian operator that acts along isopycnal surfaces (Guilyardi et al, 2001). Short-wave fluxes penetrate into the ocean based on a single exponential profile corresponding to oligotrophic water (Paulson and Simpson, 1977) with an attenuation depth of 23m (Lengaigne et al, 2007).The spectral general circulation model ARPEGE (Action de Recherche Petite Echelle Grande Echelle) is coupled to the ocean through the coupler OASIS v3 (Valcke et al, 2003). It has a horizontal resolution of 1.4° and 31 vertical levels, with resolution ranging from 10m at the surface to 70km. Deep atmospheric convection parametrization follows a mass convergence scheme (Bougeault, 1985) that uses a humidity convergence closure. Deep atmospheric convection is either triggered by low-level humidity convergence or by an unstable vertical temperature profile. Large scale precipitations are computed with a statistic precipitation scheme described by Smith (1990). Finally, surface processes are computed with SURFEX (Surface Externalisee) model (Le Moigne et al, 2009). A more detailed description of CNRM-CM5 can be found in Voldoire et al (2013).

An 800-years long control simulations is performed after a 200-years spin-up, using pre-industrial forcings, with greenhouse gases (GHG) concentrations and solar irradiance fixed to their value observed in 1850. 150 years of the 800-years control simulation OLR and wind stress daily outputs are used to characterize the modelled WWEs and their relationship with ENSO. Monthly outputs from the 800-years control simulation are used to quantify El Niño distribution and preconditioning by the equatorial oceanic heat content. In the model, we use the same definitions as in observations for defining the WWV index, El Niño amplitude and WWEs characteristics. Modelled climatologies are computed over the entire length of the control simulation. The modelled eastern edge of the warm pool is computed using the 27.5°C isotherm rather than 28.5°C in observations, because of the cold equatorial bias simulated by this model (Voldoire et al, 2013)

2.3.2 Ensemble and sensitivity experiments

In order to explore the limitations of predictability by the ocean-atmosphere system chaotic behaviour, a 100-members control ensemble simulation was run, starting from the 1^{st} April of a given year of the model simulation, with 0.1°C amplitude random white noise perturbations applied to SST to generate the ensemble. The choice of the specific model year from which this ensemble is initiated is further justified in section 4. We chose to start our ensemble on the 1^{st} of April because ECMWF ensemble forecasts in April 2014 and 2015 are similar (amplitude range and spread, see Fig. 2a,b) and include the impact of the strong WWEs that occurred in March 2014 and March 2015.

We also performed three types of sensitivity experiments to quantify the impact of WWEs on El Niño evolution. In the control ensemble, the El Niño amplitude probability distribution has reasonably converged with 50 members (not shown) and we hence use only 50 members for these sensitivity experiments. WWEs are "removed" during the model calculation by limiting positive zonal wind stress to 0.025 N.m-2 within the equatorial band (5°N-5°S, 90°E-90°W). We verified that seasonal wind stresses (defined as three-month moving averages) almost never exceed this threshold in the equatorial band in the control ensemble simulation (Fig. 3a), i.e. that this strategy efficiently removes both the stochastic and deterministic components of the wind events without affecting the large-scale low-frequency Bjerknes feedback. We performed three 50-members sensitivity ensemble simulations where "initial" (January to March), "subsequent" (April to November) and "all" (January to November) WWEs are removed. For removing initial WWEs, we proceeded as follows: there is only one strong WWE in March in the control simulation from which our ensemble starts (Fig. 3b). We ran one single member with suppressed WWEs for March, checked that the 1st of April WWV was not significantly affected, and started our 50-member ensemble from this date. Fig. 3c,d,e show the evolution of equatorial zonal wind stress for sample members of the control and three sensitivity experiments. Low-frequency westerly winds that characterize the (low-frequency) Bjerknes feedback still develop in the central/western Pacific in the "subsequent" and "all" sensitivity experiments, indicating that our approach indeed removes WWEs without affecting the lower frequency wind variability.

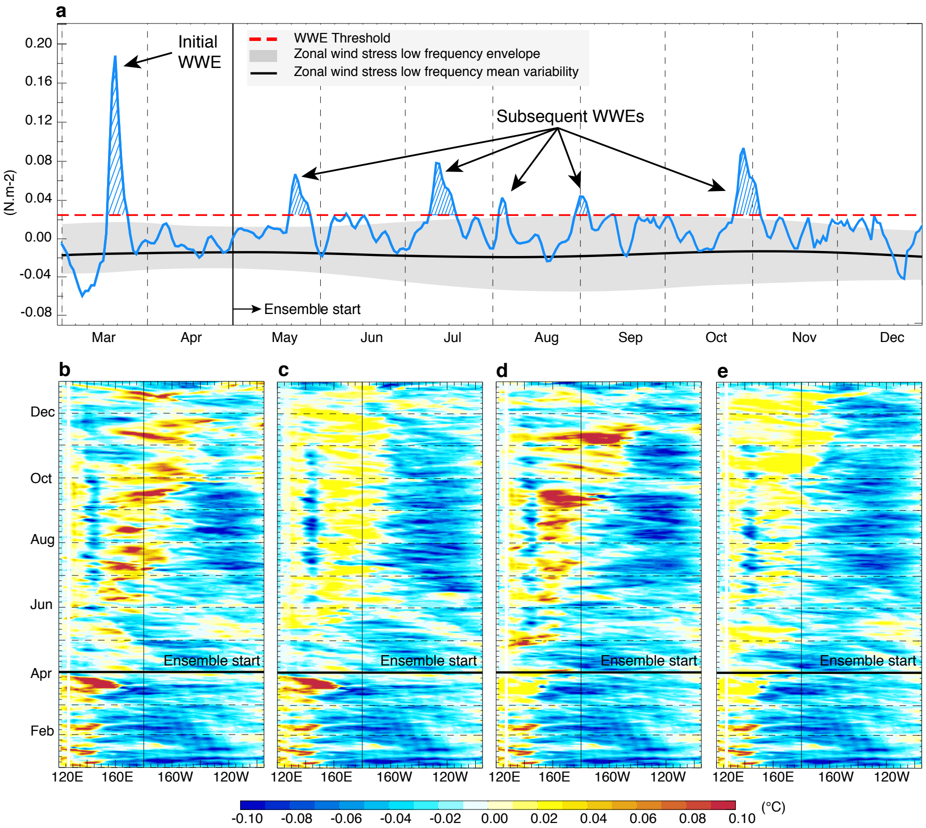

Fig. 3 **a**, Time series of the March to December zonal wind stress averaged over the [180; 160°W] region in one member of the CNRM-CM5 reference ensemble experiment (conditions before the 1st April come from the long CNRM-CM5 experiment from which the ensemble is initiated). The red line illustrates the threshold applied to remove WWEs in the "No WWE" experiments (and values above this threshold are hatched). "Initial" WWEs are defined as WWEs during January-March and "subsequent" as WWEs during April-November. Climatological (black curve) and envelope of the 1st-99th percentiles of the low frequency (90 day-smoothed, grey shading) of 2°N-2°S Pacific zonal wind stress in the CNRM-CM5 long experiment. **b, c, d, e** January to December time-longitude section of averaged [2°N-2°S] zonal wind stress from the member with the strongest warming in the Niño3 region in December for b control ensemble, c No subsequent WWE, d No initial WWE and e No WWE experiments. The low-frequency (here defined as periods >90 day) zonal wind stress variability along the equator almost never exceeds the threshold defined to remove WWEs in our experiments. I.e. WWEs are well separated in absolute zonal wind stress values from the seasonal and interannual variability, hence justifying our method for "cutting" them.

3 Model Validation

We chose the CNRM-CM5 model because it simulates the ENSO cycle and associated ocean-atmosphere feedbacks well (Bellenger et al, 2014). In particular, it accurately reproduces the El Niño amplitude distribution (Fig. 4a), with the observed distribution (50 years period) falling within the range of modelled amplitudes (whiskers on Fig. 4a were obtained from 50-years segments of the 800-years

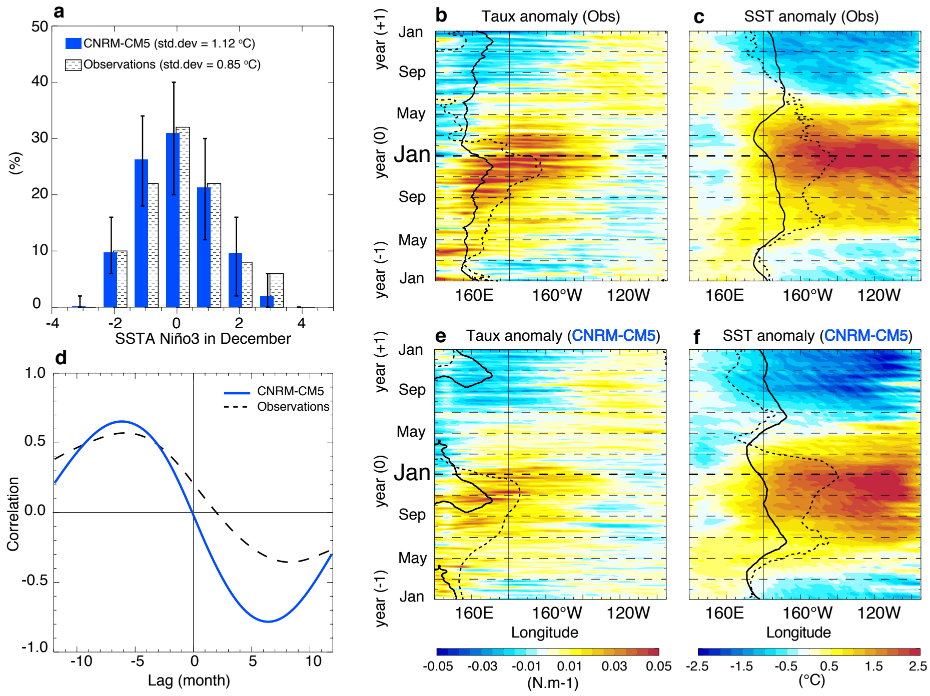

Fig. 4 **a**, Observed and CNRM-CM5 El Niño amplitude distributions. Normalized December Niño-3 SST anomaly distribution for (grey) 1966-2016 (50 years) ERSST v4 observations(Huang et al, 2015) and (blue) the 800-years CNRM-CM5 control simulation. The whiskers represent the 5-95% confidence interval on CNRM-CM5 distribution, obtained from all the 50 years segments in the 800-years simulation. The model has a good representation of El Niño amplitude distribution, considering observational uncertainties. This result stay robust when using different SST products and for every bin, the observed distribution ranges between the simulated distribution error intervals. Observed (**b, c**) and CNRM-CM5 (**e, f**) 2°N-2°S average time longitude section composite El Niño anomalies **b, e**, zonal wind stress (shading, N.m-2) and **c, f** SST (shading, °C). On panels **b** and **e**, the dashed black line represents the -0.01 N.m-2 absolute wind stress contour composite (i.e. western edge of equatorial easterlies) and the thick line its climatological value. On panels **c** and **e**, the dashed black line represents the warm pool eastern edge composite (see methods) and the thick line its climatological value. **d** Lagged correlation between the 5-month running-mean Niño-3 SST anomaly and the 5-month running-mean WWV anomalies in the observations (dashed) and the 800-years CNRM-CM5 control simulation (blue). On panel **d**, WWV anomalies lead Niño-3 SST anomalies.

long control simulation). It also reproduces the space-time evolution of equatorial zonal wind stress (Fig. 4b,e) and SST anomalies (Fig. 4c,f) associated with El Niño. As in the observations, early westerly wind anomalies induce an eastward shift of the warm pool and weak central Pacific positive SST anomalies in boreal spring (Fig. 4b,e). The SST and westerly wind anomalies grow through summer to reach a peak at the end of the year and generally evolve towards a La Niña state during the following boreal spring. The composite SST anomalies have comparable amplitudes in the model and observations, with up to 2.5 °C warming in December in the eastern Pacific (Fig. 4c,f). The low-frequency westerly wind response is however underestimated in the model (Fig. 4b,e). This is a recurrent bias of ocean-atmosphere coupled models, which tend to underestimate the Bjerknes feedback

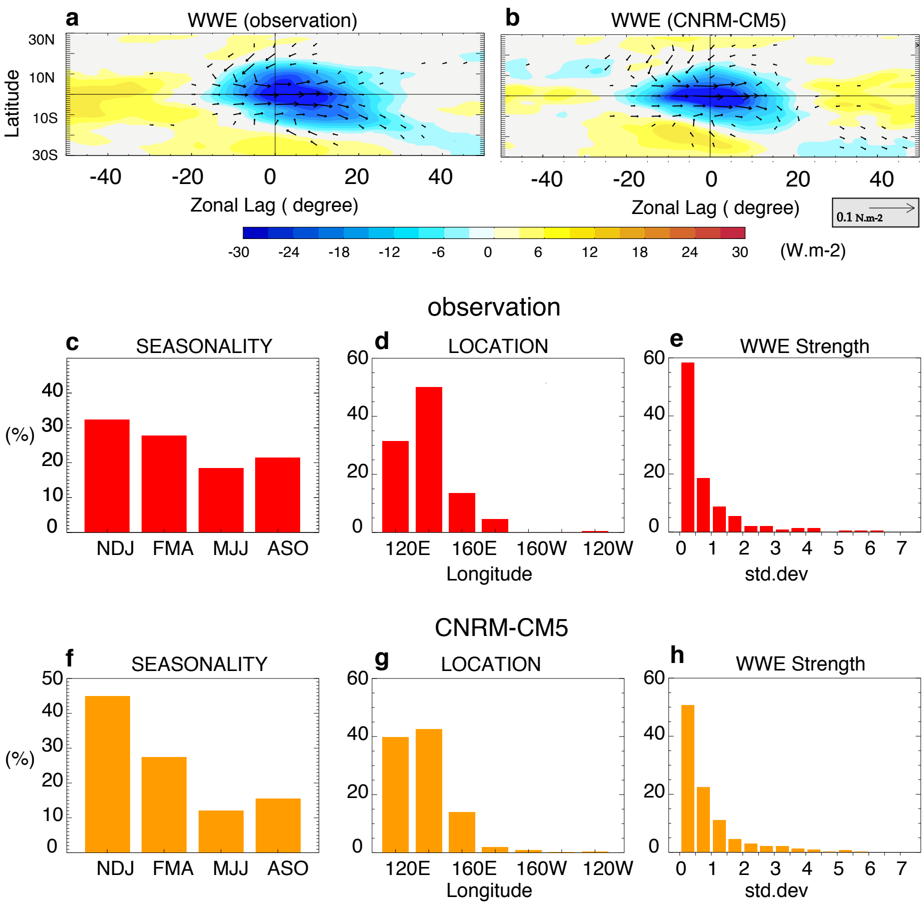

Fig. 5 **a** Observed and **b** modelled Spatial composite of WWEs wind stress (vectors, N.m-2) and outgoing long-wave radiation (shading, W.m-2) intraseasonal (5-90 days filtered) anomalies. The composites are centred on WWEs central dates and longitudes. Observed (**c,d,e**) and modelled (**f,g,h**) WWEs **c,f**, seasonal **d,g**, longitudinal and **e,h**, strength (see methods) distributions.

(Guilyardi, 2006; Bellenger et al, 2014). In addition to low frequency dynamics, this bias may affect the influence of WWEs on ENSO by limiting the large-scale amplification of WWE-induced SST anomalies and hence preventing the occurrence of subsequent WWEs. The El Niño preconditioning through enhanced WWV is relatively well simulated in the model, with positive WWV anomalies leading El Niño by about 6 months (negative lags on Fig. 4d). The unrealistic negative correlation for positive lags on Fig. 4d is also a common bias of the ocean-atmosphere coupled models that tend to produce a too symmetric ENSO cycle (skewness of Nino-3 SST interannual anomalies equal to 0.4 in the model in comparison to 0.8 in the observation, Zhang and Sun, 2014).

The confidence in the model results discussed below strongly relies in the ability of the model to capture WWEs essential characteristics and their relationship with low-frequency SST anomalies. Fig. 5 compares the characteristics of observed and

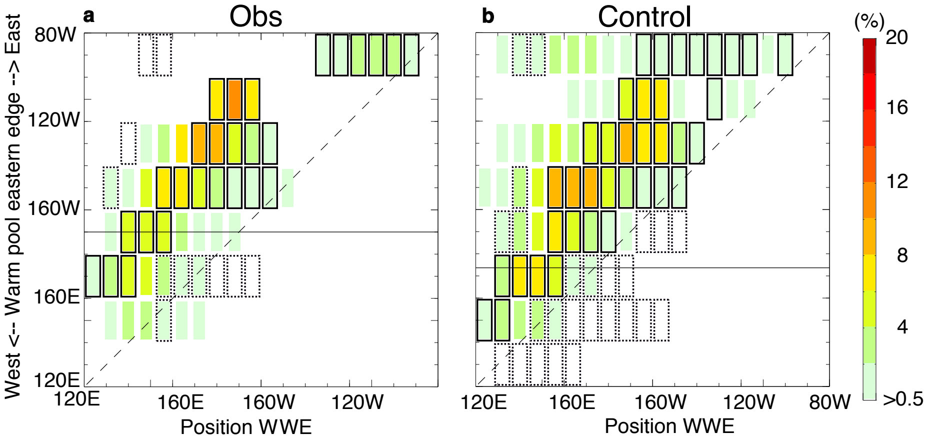

Fig. 6 **a, b** Zonal distribution of the WWE occurrence probability (%, see text for details), as a function of the position of the eastern edge of the Warm pool for (**a**) observations and (**b**) the model. Black solid (dashed) boxes represent bins where the wind event occurrence probability is significantly higher (lower) than what would be expected with a random distribution at the 95 % confidence level. The horizontal black line indicates the warm pool eastern edge mean position.

modelled WWEs following Puy et al (2015). Both observed and simulated WWEs are characterized by increased deep atmospheric convection (i.e. negative OLR anomalies) and by a zonal and meridional extension of about 40° and 20° respectively (Fig. 5ab). The modeled WWEs are modulated by equatorial atmospheric Rossby waves and the Madden-Julian Oscillation (Puy, 2016), in agreement with observations (Puy et al, 2015). Observed and modelled WWEs occur preferentially in boreal winter (Fig. 5c,f) in the western Pacific (Fig. 5d,g). The long positive tail of the observed WWEs strength distribution is also well captured by the model (Fig 5e,h). This is an important aspect of the WWEs characteristics, since the occurrence of exceptionally strong WWEs such as the one in March 1997, have been suggested to have a particularly strong impact on El Niño evolution (Lengaigne et al, 2004a).

A proper model representation of the observed modulation of WWEs probability by the warm pool zonal displacement (i.e. the WWEs deterministic component) is of particular importance for the present study. Fig. 6 assesses this relationship in both observations and model by showing the zonal distribution of the WWEs occurrence probability, as a function of the position of the eastern edge of the warm pool (i.e. a quantification of the eastward expansion of the warm pool) for the observations and the model. The WWEs occurrence probability is computed as the ratio of the total duration of WWEs for a given longitude and position of the WPEE to the total number of days for which the WPEE is at this longitude. In both cases, the highest probability for WWEs occurrence shifts eastward along with the warm pool. More quantitatively, the WWEs probability of occurrence is multiplied by up to 20 in the central Pacific when the warm pool is shifted eastward beyond 160°W. The WWEs deterministic component (i.e. their occurrence probability modulated by WPEE east-west displacements) is hence also very well captured by this model.

4 Linking El Niño amplitude to WWEs activity

As discussed above, early 2014 and 2015 were very similar in terms of equatorial oceanic and atmospheric preconditioning. First, the WWV in early 2014 and 2015 was also anomalously high (1.4 standard deviation as in early 1997 (Fig. 1a)). These two years were also characterized by a series of early-year WWEs (Fig. 7d,g), which were one of the strongest on record (a cumulative strength of 7.3 standard deviation in 2014 and 5.6 standard deviation in 2015), comparable to the one in 1997 (cumulative strength of 6, Fig. 7a). These WWEs shifted the warm pool eastward (Fig. 7b,e,h) and triggered downwelling Kelvin waves that deepened the thermocline in the eastern Pacific (Fig. 7c,f,i).

In this section, we further investigate the role of high frequency wind forcing (WWEs and EWEs) in promoting an extreme El Niño in the model for a situation comparable to that observed in early 2014 and 2015. We first identified in the control simulation an analogue to the equatorial Pacific conditions observed in early 2014 and 2015. We defined this analogue as a model background state having similar March WWV anomalies and January-March cumulative WWE strength to those observed in early 2014 and 2015 (Fig. 8). Fig. 8a,b is similar to Fig. 1a,b but for a 35-years chunk of the long control simulation. This analysis led us to select the model year 2154 as it exhibits an initial WWE strength of about 6 standard deviation (compared to 5.6 and 7.3 in 2015 and 2014 respectively; Fig. 8c) and WWV anomaly reaching 1.4 (as in 2014 and 2015, Fig. 8d).

However, if the WWV quantifies the recharge state of the equatorial Pacific, it doesn't precisely account for the spatial structure of the subsurface temperature anomalies. While March 1997 and 2014 both exhibit warm subsurface anomalies confined to the central Pacific near the dateline, March 2015 and the model initial conditions show shallower warm anomalies located further east and sloping upwards in the eastern Pacific (not shown). These subtle differences in initial subsurface temperature anomalies are not encompassed by the WWV index, which is an integrated measure over the entire equatorial band. This may play a role in the subsequent Pacific evolution but this is out of scope of the present study.

Off-equatorial SST anomalies in the tropical Pacific have also been suggested to play a role in the development of El Niño (Chang et al, 2007; Zhu et al, 2016; Min et al, 2015). Observations in March 2015 in the north Pacific are reminiscent of the north Pacific meridional mode (Fig. 9 a) discussed in Chang et al (2007) but this pattern is weaker in March 1997 and 2014 (Fig. 9 b,c) and absent in the model initial conditions (Fig. 9 d). Similarly, observations in March 2014 and 2015 display negative SSTA in the south-eastern Pacific (Fig. 9 bc), consistent with the South Pacific Meridional mode suggested by Min et al. (2013), but such anomalies are absent in March 1997 and our initial conditions (Fig. 9 a,d).

The experimental framework used in the present study is designed to focus on two equatorial El Niño precursors (i.e. WWV and early-year WWEs) which were similar in early 2014 and 2015. It does not allow, however, to test the potential influence of off-equatorial SST precursors or the spatial structure of the subsurface temperature anomalies on the evolution of El Niño.

A 100-members ensemble simulation is run from small perturbations applied to this 2014 and 2015 analogue initial state on the 1st of April (see section 2), i.e. after that the early-year strong WWE has shifted the warm pool eastward and seeded the potential for more WWEs. The El Niño amplitude ensemble diversity is

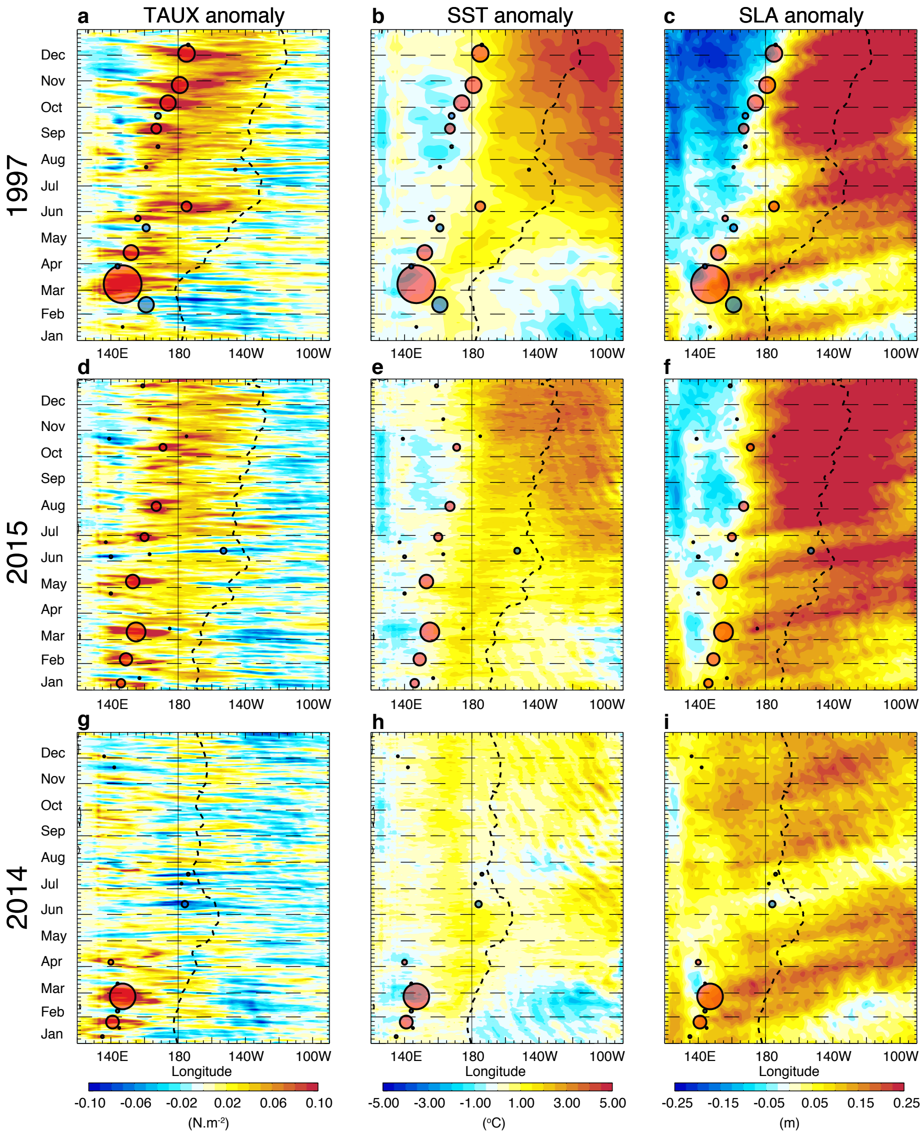

Fig. 7 Averaged 2°N-2°S time-longitude section of observed **a**, Zonal wind stressKumar et al (2013) **b**, SST(Reynolds et al, 2002) and **c**, sea surface height (a proxy for thermocline depth, http://www.aviso.altimetry.fr/duacs/) anomalies during 1997. **d, e, f**, Same for 2015. **g, h, i**, Same for 2014. The dotted black contour indicates the eastern edge of the western Pacific Warm Pool (defined as the 28.5 °C isotherm). On all panels, WWEs (red circles) and EWEs (easterly wind events, blue circles) have been added. The size of the circles that indicate the wind events central dates and longitudes is proportional to the wind event strength.

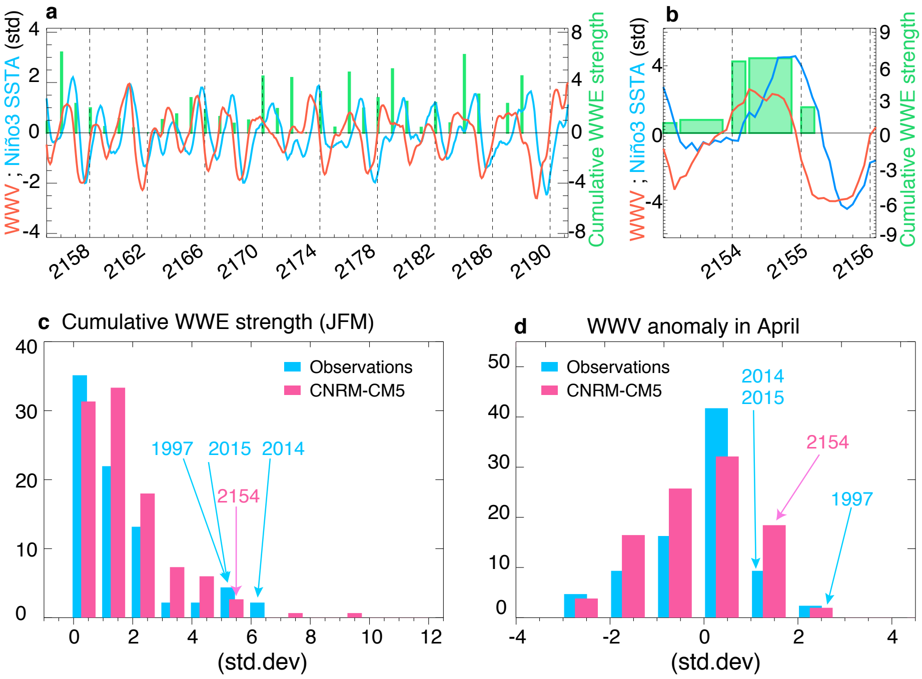

Fig. 8 **a**,**b**, Similar to Fig 1a,b but for 30 years of the control simulation. Amplitude distribution of **c**, January-March cumulative "initial" WWE strength (see methods) and **d**, March WWV in (blue) observations and (pink) model. On both panels, the observational values of those parameters for 1997, 2014 and 2015 and chosen model year 2154 are indicated.

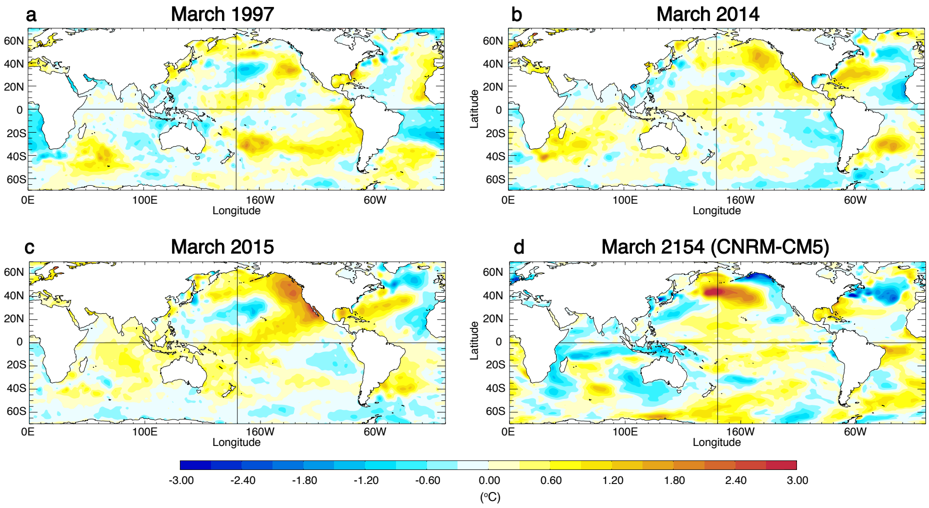

Fig. 9 Monthly average SST anomaly during March (a) 1997,(b) 2014, (c) 2015 and (d) modelled year 2154. The product HadISST is used for the observations (Rayner et al, 2003).

hence uniquely due to the now-famous butterfly effect (Lorenz, 1993, i.e. sensitivity to initial conditions). Fig. 10 however illustrates that this chaotic behaviour does not preclude predictability for early spring forecasts of El Niño's peak at 9 months lead times. The ensemble El Niño amplitude probability distribution function is indeed very different from that of the 800-yr long reference experiment (Fig. 10b), indicating El Niño predictability (Stockdale et al, 1998) from initial conditions such as those of early 2014 or 2015. The positive WWV anomalies and early-year WWEs indeed preclude the occurrence of a La Niña, with end-of-year conditions that range from a nearly neutral state to extreme El Niño in both ECMWF forecasts and our model framework (Fig.2a,b and Fig. 10a).

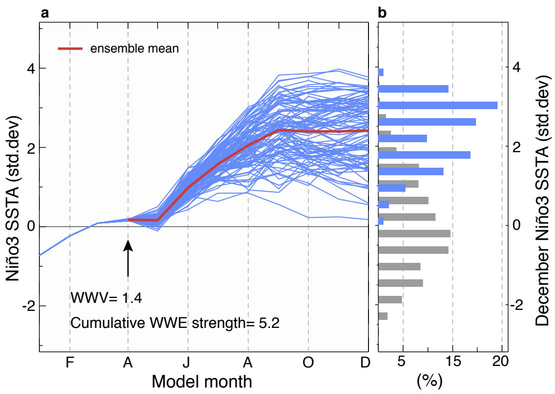

Fig. 10 **a**, January to December standardized Niño-3 SST anomaly evolution for 100 members of the CNRM-CM5 ensemble run with a similar initial state to that in 2014 and 2015, in terms of the main precursors of El Niño: early-year WWV and WWEs cumulative strength, and **b**, corresponding December standardized Niño-3 SST anomaly distribution (blue). The December standardized SST anomaly distribution for the 800-years long CNRM-CM5 simulation (grey) is also shown on panel **b**. The red line on panel a represent the ensemble mean.

Fig. 11 suggests that the initial WWE strongly contribute to the El Niño amplitude, as indicated by previous studies (Lengaigne et al, 2004a; Fedorov et al, 2015; Lengaigne et al, 2002; McPhaden et al, 2006b). The strong initial March WWE forces a downwelling Kelvin wave, whose related eastward current anomalies induce an eastward displacement of the warm pool and central Pacific warming during April in all the ensemble members (Fig. 11). The oceanic impact of this initial WWE is consistent with the observations in early 1997, 2014 and 2015 (Fig. 7). After this common initial evolution, there is a clear divergence between ensemble members, some of which evolve into extreme El Niños and others into weaker El Niños (Fig. 11). The composite of the ten members that show the largest warming in the Niño3 region in December are of course associated with larger eastern and central Pacific SST anomalies and eastward expansion of the warm pool (Fig. 12b). But they are also associated with more frequent and intense subsequent WWEs, especially during summer (Fig. 12ab), as in 2015 (Fig. 7d). The ten strongest simulated El Niños are indeed associated with twice as many summer WWEs than the ten weakest El Niño (6/year compared to 3/year, Fig. 12ab). Strong El Niños are not only associated with more WWEs but with a

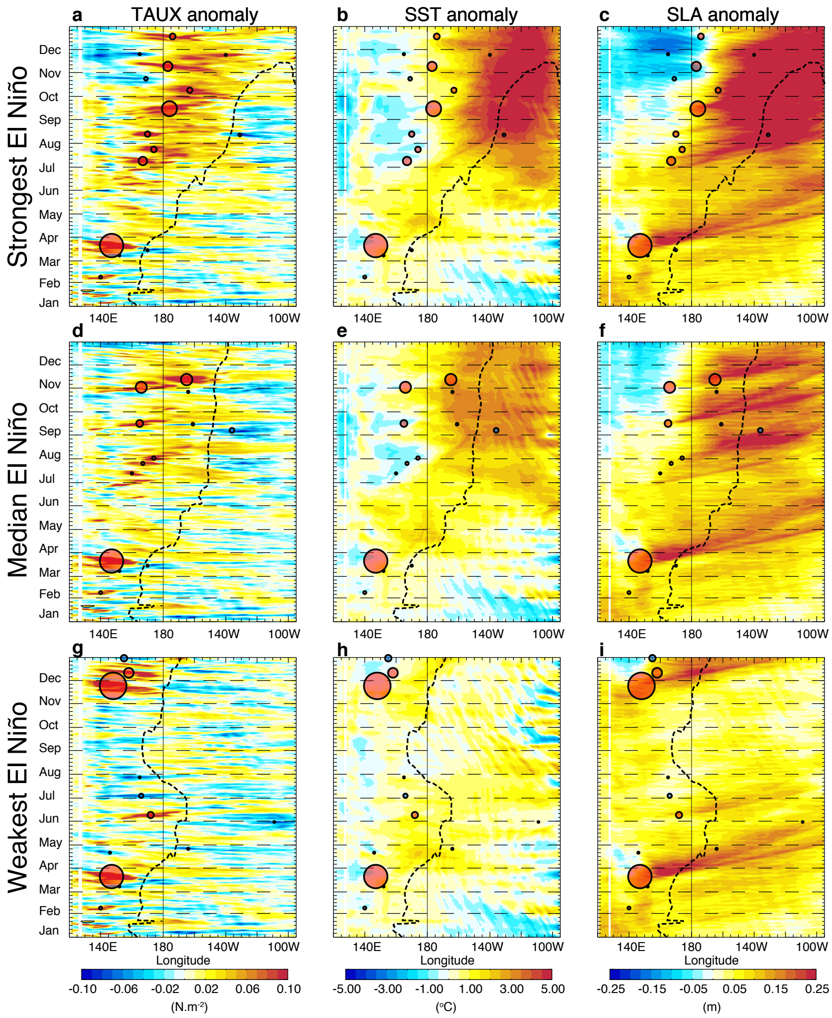

Fig. 11 Comparison between extreme,moderate and weak warming events in CNRM-CM5 ensemble simulation. As Figure. 5, but for three members of the CNRM-CM5 reference ensemble that produce qualitatively similar evolutions to those in **a, b, c**, 1997 (strongest warming in the model November-January ensemble Niño-3 SST anomaly); **d, e, f**, 2015 (the median warming); **g, h, i**, 2014 (the weakest warming). The dotted black contours indicate the eastern edge of the western Pacific Warm Pool (defined as the 27.5 °C isotherm, see methods). On all panels, WWEs (red circles) and EWEs (easterly wind events, blue circles) have been added. The size of the circles that indicate the wind events central dates and longitudes is proportional to the wind event strength.

larger cumulative WWEs strength. There is indeed a strong linear relationship (0.72 Pearson correlation, $p<0.01$) between the cumulative strength of subsequent (i.e. April to November) WWEs and the eastward expansion of the warm pool (i.e. measured as the location of the warm-pool eastern edge) in December across the ensemble (Fig.12d). A similar correlation is found between the cumulative strength of subsequent WWEs and the Niño-3 SST anomaly in December (0.7, Fig. 13).

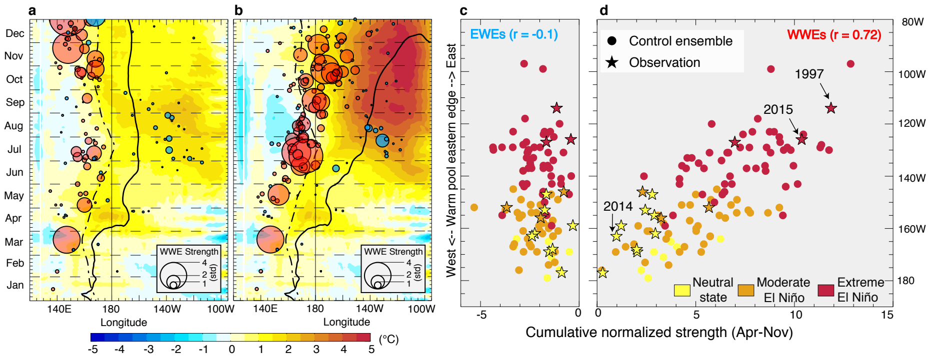

Fig. 12 a,b, Composite time-longitude section of 2°SN-2°SS-averaged SST anomalies for the 10 weakest and 10 strongest El Niños in the CNRM-CM5 control ensemble experiment. Red (blue) circles indicate the WWEs (EWEs) central dates and longitudes for all the members in each composite, the size of the circle being proportional to the WWE strength (see methods). The black line on panels a,b indicates the eastern edge of the western Pacific warm pool and its climatological position (dash-dotted line). c, d Scatter plot of the December Pacific Warm pool eastern edge position versus the April to November cumulative (c) EWEs and (d) WWEs strength (see methods) for (dots) each of the 100 members of the CNRM-CM5 ensemble control run and (stars) from observations with the colour indicating the El Niño category (yellow for neutral state, orange for moderate and red for extreme El Niños)

The observed 1997 and 2015 El Niños align with some of the most intense El Niños and subsequent cumulative WWE strength in our experiment (Fig. 12d). As a comparison, the magnitude and evolution of El Niño in the member associated with the warmest SST anomaly in the Niño3 region bears strong similarities with the observed 1997 El Niño (i.e, a series of strong WWEs in summer and fall associated with the rapid eastward shift of the warm pool and SST anomalies reaching 5°C in the eastern Pacific, Fig. 11a,b,c and Fig. 7a,b,c). A similar comparison can be done with the median El Niños in our ensemble and the observed 2015 El Niño, both associated with a series of strong WWEs in summer and fall (weaker than in 1997 though) and the rapid eastward shift of the warm pool and SST anomalies reaching 3°C in the eastern Pacific (Fig. 11d,e,f and Fig. 7d,e,f). On the other side of the distribution, the observed weak 2014 event lies at the lower end of this relationship, in line with studies suggesting that the 2014 El Niño was linked to an absence of summer WWEs (Menkes et al, 2014). Indeed, the member associated with the weakest El Niño exhibits weak SST anomalies in the central/eastern Pacific (< 1°C) and a reduced WWEs activity in summer/fall following the strong initial (Fig.12a and Fig. 11g,h,i) as in 2014 (Fig. 7g,h,i).

We will now explore during which period of the forecast WWEs occurrence influences most the El Niño amplitude at the end of the year. Fig. 13 shows the correlation between the December Niño-3 SST anomaly (i.e. El Niño amplitude at its peak) and cumulative WWEs strength integrated progressively over longer periods between April and November. There is a large increase in correlation (from 0.15 to 0.6) when including June, July and August in the averaging period, and a stabilization afterwards. This suggests that WWEs occurring during the June-August period (i.e. boreal summer) are critical to set the El Niño amplitude at the end of the year (this results is further confirmed in section 5).

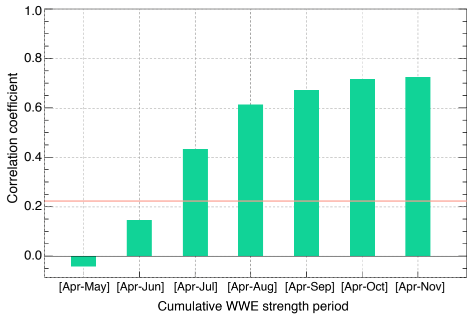

Fig. 13 Correlation coefficient between the cumulative WWEs strength and Niño3-SSTA in December for the 100 members of the control ensemble simulation as a function of the period used to cumulate the WWEs strength. The red line represent the 99% of significance (t-test) threshold.

We have demonstrated above a strong statistical link between April-November cumulative WWE strength (with June and July contributing most) and the El Niño peak amplitude. Previous studies (Hu and Fedorov, 2016; Levine and McPhaden, 2016) have also suggested that a series of EWEs in June and July (Fig. 7g) could have halted the 2014 El Niño on its way. Yet, some strong EWEs occur in July in some of the members with the ten largest El Niños in our simulation (Fig. 12b). Symmetrically, there are members in our control ensemble which do not develop EWEs, but end up producing a weak El Niño (not shown). The scatterplot between the April-November cumulative EWEs strength and the El Niño amplitude shown in Fig. 12c further indicates that there is no significant correlation between the EWEs activity and El Niño amplitude in neither our ensemble nor observations. In our ensemble simulation, there is hence a much stronger statistical relationship between El Niño amplitude and WWEs than with EWEs (0.7 vs. -0.1 correlation, Fig. 12cd). This of course does not preclude that some EWEs may play a role in specific ensemble members, but suggests that their role is not as systematic as those of WWEs. We will come back to this in the discussion section.

5 Necessary conditions for extreme El Niño events

This statistical relationship between WWEs activity and El Niño amplitude does not reveal if WWEs only passively respond to warm pool displacements, or if they actively participate to El Niño growth. To investigate this, an additional ensemble is performed in which subsequent WWEs were artificially removed (hereafter called "no subsequent WWEs" ensemble - see section 2 for details). Fig. 14a,b compares the evolution and December values of Niño3 SST anomalies of the control and "no subsequent WWEs" ensembles. As seen earlier for the control simulation (Fig. 11), the "initial" WWE forces a downwelling Kelvin wave which induces an eastern Pacific warming from May to early July in both ensembles (Fig. 14a). From July onwards, however, the two ensemble mean start diverging. The mean Niño3 SST of the "no subsequent WWEs" ensemble continues warming for two more months, but then stalls and even decays after September. This confirms the prominent impact of the subsequent WWEs occurring in summer, as suggested by Fig. 13.

One should however not only focus on the ensemble mean, as El Niño forecasts need to be considered as probabilistic forecasts. Fig. 14b hence further compares the probabilities for neutral, moderate or extreme ENSO state in the control and "no subsequent WWEs" ensembles. Subsequent WWEs strongly enhance the odds (54% vs. 10%) of a 2015-like extreme El Niño and reduce those of a 2014-like weak El Niño (30% vs. 8%, Fig. 14b).

To investigate the role of the initial WWEs in the evolution of El Niño in 2014 and 2015, a similar experiment is performed with the influence of the March WWE removed in the initial conditions (hereafter called "no initial WWEs" ensemble; see section 2). Unlike the "no subsequent WWEs" ensemble, the ensemble mean of the "no initial WWEs" and control ensembles start diverging in May, revealing the strong impact of the initial March WWE on eastern Pacific SST (Fig. 14c). While subsequent WWEs continue to induce a rise in the ensemble-mean Niño3 SST until the end of the year in the "no initial WWEs" ensemble, it never catches up with the control ensemble, indicating the strong impact of the initial WWE on the peak El Niño amplitude. The occurrence of strong initial WWEs indeed significantly favours the advent of extreme El Niño events (54% against 18%) and prevents weak 2014-like El Niños (34% vs. 8%, Fig. 14d).

A last experiment is finally conducted where both the initial and the subsequent WWEs are removed (hereafter called "no WWEs" ensemble, Fig. 14e,f). In this experiment (as in "no subsequent WWEs"), the "intraseasonal Bjerknes feedback" (tendency for WWEs to induce an eastward displacement of the warm pool and more WWEs) has been suppressed. The "initial kick" of the March WWE has also been suppressed, with the recharged WWV providing the only El Niño-favourable initial condition. The preconditionning by a recharged WWV still favors a warming at the end of year without the occurence of WWEs (Fig. 14e), which is purely the result of the classical "low-frequency" Bjerknes feedback. However, the occurrence of an extreme El Niño such as that in 2015 is nullified in this ensemble and a weak-borderline 2014-like El Niño become almost six times more likely (46% against 8%,Fig. 14f). This clearly shows that sustained WWEs throughout the year are a necessary condition for extreme El Niños in that model.

In observations, the three recent extreme El Niños all occurred after a recharged oceanic state and intense WWE activity (Fig. 1a). The results above demonstrate that when the equatorial Pacific is initially recharged, sustained WWEs are necessary to yield an extreme El Niño. Is a recharged initial state also necessary for the development of an extreme El Niño? In the long-control run, a strong WWE activity throughout the year is also a necessary condition for extreme El Niños to occur, whatever the early-year recharge state (Fig. 15a). In this figure, "No or weak (resp. strong) WWE" characterize the years with WWEs strength less or equal to (resp. larger than) one standard deviation and the discharged, neutral and recharged states are respectively defined as January-March WWV anomalies below -0.75, between -0.75 and 0.75 and above 0.75 standard deviation. While a recharged state excludes the occurrence of a La Niña, a strong WWE activity is also necessary to obtain an extreme El Niño (Fig. 15a). Extreme El Niños can also occur following a neutral state and intense WWEs but this is very rare in our experiments (5% versus 22% for a recharged state and strong WWEs and 4% when all cases were considered, Fig. 15a). In the long-control simulation, initial WWEs are also efficient in triggering extreme El Niño events (Fig. 15b), with all extreme El Niño being preceded by a strong WWE activity in JFM. More gener-

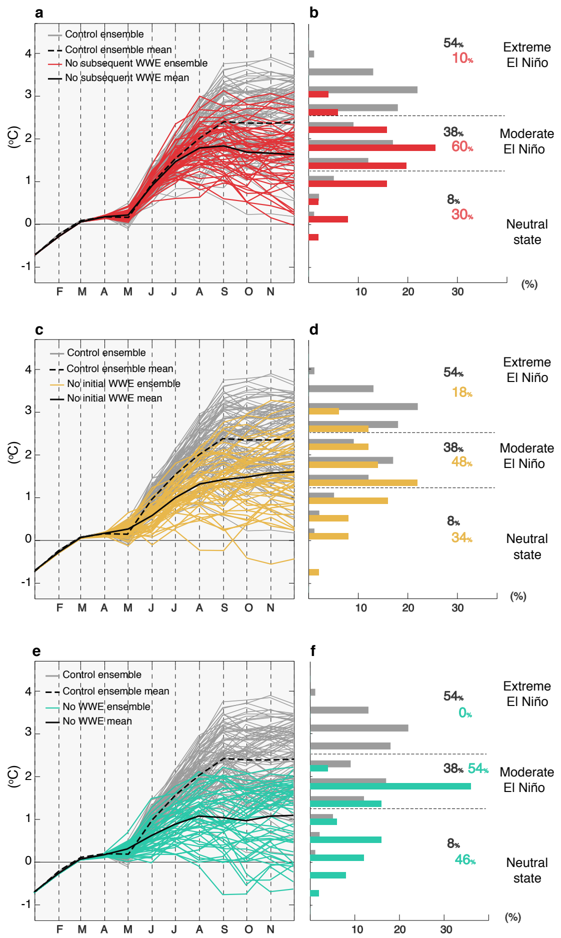

Fig. 14 **a, c, e** January to December Niño-3 SST anomaly evolution for the first 50 members of the (grey) control ensemble run, (red) No "subsequent" WWE, (gold) No "initial" WWE and (teal blue) No WWE sensitivity experiments. **b, d, f** corresponding December Niño-3 SST anomaly distribution for the 50 members of the (grey) control ensemble run, (red) No "subsequent" WWE, (gold) No "initial" WWE and (teal blue) No WWE sensitivity experiments. On **b, d, f**, the percentage of each El Niño categories have been added. On **a, c, e** the solid black line indicates the corresponding ensemble mean and the dashed black line the control ensemble mean.

ally, the WWE activity tends to shift the El Niño amplitude towards higher values for recharged and neutral states, but has little impact for discharged states (Fig. 15a)

This weakened impact of WWEs on El Niño during discharged state is likely due to the fact that the tendency for an initial WWE to induce successive ones also depends on the oceanic background state. When the Pacific is initially recharged, an initial WWE makes the occurrence of more WWEs later in the year 2.5 times more likely (Fig. 15c), in agreement with the results presented above and suggested in the observations (Lengaigne et al, 2004a). However, this relationship is modified

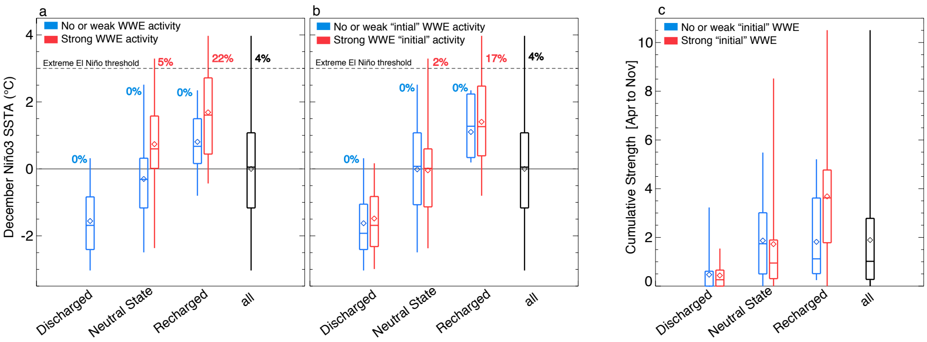

Fig. 15 a, Average December Niño3 SST anomalies when the "initial (January-March) and "subsequent (April-November) WWE activity is (blue) weak or (red) strong for 3 initial (January-March) recharge state of the Pacific ocean in the CNRM-CM5 control simulation (see text for further details). b, Average December Niño3 SST anomalies when the "initial" (January-March) WWE activity is (blue) weak or (red) strong for 3 initial (January-March) recharge state of the Pacific in the CNRM-CM5 control simulation. On panels a and b, the average December Niño3 SST anomalies during all recharge and WWE activity conditions is also shown in black. c, Average standardized cumulative WWE strength for April-November when the initial WWE activity (January-March) is (blue) weak or (red) strong for 3 initial (January-March) recharge state of the Pacific in the CNRM-CM5 control simulation (see text for further details). On all panels, the boxes (whiskers) give the 1st, 25th, 75th, 99th percentiles and the median of the distributions. The percentage of extreme El Niño (see method for further detail) for each categories are also given. On panel a, the distribution of December Niño3-SSTA for discharged state and strong WWE activity is not given because 0 year satisfied those criteria in the control simulation.

when the Pacific exhibits neutral or discharged conditions, with a weaker impact of initial WWEs on the subsequent WWEs activity in neutral conditions (1.5 times more likely) and no impact when the Pacific is discharged (Fig.15c). In this figure,"No or weak (resp. strong) initial WWE activity" on Fig. 15c characterize the years with initial (i.e. Jan to March) cumulative strength less or equal to (resp. larger than) one standard deviation. Overall, once an early year WWE has occurred in presence of elevated WWV, this enhances the odds for an extreme El Niño (Fig. 15a). This positive feedback between initial and successive WWEs is reduced in presence of a neutral state, and nullified in a discharged state, hence reducing (or altogether cancelling) the odds for an extreme El Niño.

6 Summary and Discussion

The strongest El Ninos on record were preceded by anomalously high upper ocean heat content combined with exceptionally strong westerly wind variability. Similar conditions evolved into a weak El Niño in 2014 and forecasts failed to predict the peak amplitude of this event. Similar conditions also occurred in 2015, which turned into a record-breaking event by the end of the year. Why did similar equatorial conditions in early 2014 and 2015 evolved so differently? Unpredictable wind variability could be responsible for the 2014 El Niño failure (Hu and Fedorov, 2016; Zhu et al, 2016; Menkes et al, 2014) and the advent of the extreme event in 2015 (Hu and Fedorov, 2017). Unlike in 2015 and 1997, the summer and fall WWE activity was indeed not as strong in 2014 (Fig. 7d,g). WWEs have a deterministic component: they are more likely when the western Pacific warm pool extends anomalously eastward (Eisenman et al, 2005; Gebbie et al, 2007; Lengaigne et al, 2003; Puy et al, 2015). This relationship, however, remains probabilistic: an abnormally warm central Pacific favors more WWEs than usual, but there is still a probability that less WWEs than usual may occur. In this study, we tested the hypothesis that intrinsic WWEs stochasticity could explain the differences between 2014 and 2015 El Niño evolutions. We also investigated conditions conducive to extreme El Niños: are early-year intense WWEs and recharged upper ocean heat content as observed prior to exceptionally strong El Niños always necessary?

We used the CNRM-CM5 coupled ocean-atmosphere model because it reproduces the ENSO cycle, its preconditioning by WWV, WWEs characteristics and the influence of the warm pool displacements on WWEs quite exceptionally for a CGCM (Section. 3). Our ensemble simulations show that despite their deterministic behaviour, WWEs still display a sufficiently strong stochastic component to explain the different 2014 and 2015 evolutions, consistently with the findings of Larson and Kirtman (2015). Although early-year strong WWEs and elevated WWV preclude the occurrence of La Niña events, El Niño amplitude ranges between weak 2014-like (with few WWEs) to extreme 2015-like El Niño events (with many WWEs). We showed that the diversity of El Niño magnitude is linearly related to the cumulative WWEs strength (a metric that characterize the WWEs activity) from April to November, with WWEs occurring in June-July contributing most. We further ran sensitivity ensemble experiments starting from the same initial conditions as above, but with WWEs filtered out (Fig. 16a). Extreme El Niños become five times less likely if summer and fall WWEs are artificially suppressed and three times less likely when initial WWEs are removed. No extreme El Niño occur in the sensitivity ensemble experiment when all WWEs are removed. A weak El Niño such as in 2014 was not unlikely in ECMWF forecasts (29%, Fig. 16b) but our experiments show that such a weak event becomes almost four times more likely if no initial or subsequent WWEs occur and five time more likely when both initial and subsequent WWEs are absent. These results confirm the hypothesis of Menkes et al (2014) who suggested, using forced oceanic simulations, that the lack of summer WWEs could explain the stalled 2014 El Niño progression.

The long control simulation allowed us to further investigate necessary conditions for the development of extreme El Niños for various contexts, different than the 2014 and 2015 El Niños. In this simulation, extreme El Niños never occur when the equatorial Pacific is initially discharged. We also showed that they occur very rarely after a neutral state (only 2.4% of the cases when a strong WWE activity is also present throughout the year), in line with precedent studies (Fedorov et al, 2015). Extreme El Niños become the most frequent when the equatorial Pacific is initially recharged, but only when a strong WWE activity is also present throughout the year, in which case they occur 17.8% of the time (corresponding to 4.5 times more likely compared to the probability of occurrence of an extreme El Niño considering all cases). We also confirmed that an early-year WWE increases the probability of subsequent WWEs later in the year, as suggested in the observations. This effect is however more efficient when the equatorial Pacific is initially recharged. We speculate that this is due to the fact that recharged states are associated with a warm pool that extends further eastward, favouring subsequent WWEs. Recharged states are also associated with a more intense zonal sea surface

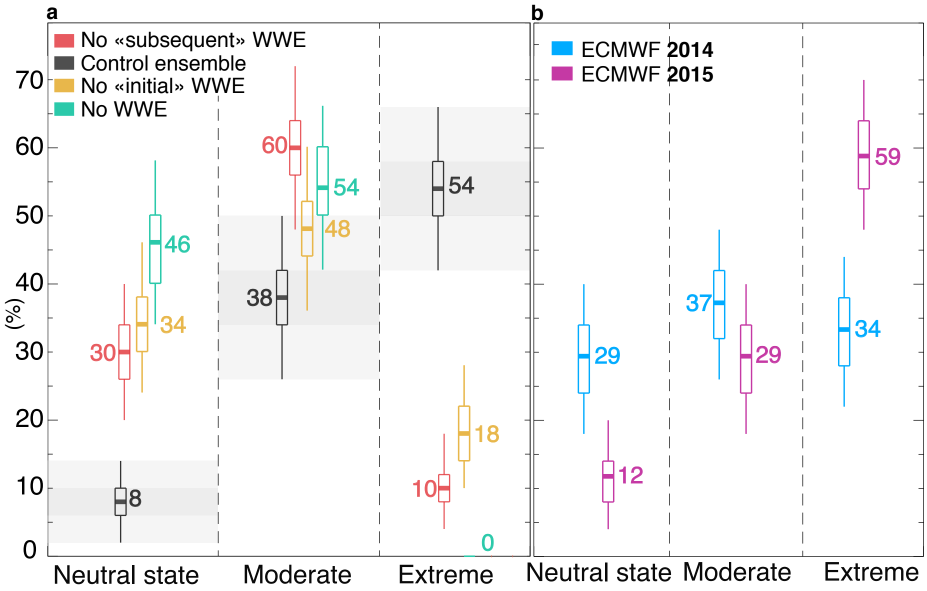

Fig. 16 a, Percentage of neutral state, moderate and extreme El Niños in the CNRM-CM5 2014/15-like ensemble experiment (black) and for experiments where subsequent (April to November, red), initial (January to March, gold) and all Westerly Wind events (teal blue) are artificially suppressed (see methods) and (b), ECMWF 1st of April 2014 (light blue) and 2015 (purple) operational forecasts. The boxes (whiskers) give the 25 and 75 (5 and 95) % confidence intervals (see methods), and the grey shading on panel (a) displays this confidence interval for the control ensemble.

temperature gradient in the central Pacific which lead to a stronger SST response to a given WWEs (Puy et al, 2016), and hence is more efficient to shift the warm pool further eastward.

The potential impact of a series of EWEs halting the 2014 El Niño during its development has also been suggested (Hu and Fedorov, 2016; Levine and McPhaden, 2016). Yet, there was a similar EWE in June 2015 (Fig.7d,g) that did not stop the developing El Niño. Also, unlike for WWEs, we found no significant correlation between summer/fall EWEs activity and El Niño amplitude in neither our ensemble nor observations (Fig. 12c). This indicates that the impact of EWEs on El Niño amplitude may be model-dependent (no impact in our model, an impact in (Hu and Fedorov, 2016; Levine and McPhaden, 2016)). More studies with other coupled models are hence probably needed to ascertain whether the summer 2014 EWEs did indeed stop the El Niño on its way. Overall, our study does not exclude an EWE having played a role in 2014, but suggests that the effect of EWEs on El Niño is not systematic (as opposed to WWEs). Our alternative (but not necessarily exclusive) explanation simply relates the uncertainty in El Niño amplitude forecasts to the WWE stochastic component: a moderate El Niño was more likely in 2014, but nature followed the less likely option in which few WWEs and a weak El Niño occurred.

Due to its state-of-the-art oceanic and atmospheric initialization (Balmaseda et al, 2013) and ensemble generation methods (Weisheimer et al, 2014), the ECMWF ensembles take into account the differences between 2014 and 2015 early-year initial conditions. April 2014 forecasts predicted almost equally likely odds for a 2014-like weak (29%), moderate (37%) or extreme (34%) El Niño (Fig. 16b). There is however a clear tendency for the April 2015 ECMWF forecast distribution to be shifted towards higher El Niño amplitude relative to that of 2014, with significantly more chances for an extreme El Niño in 2015 (59%), and less for no El Niño (12%, Fig.16b). This change in the El Niño amplitude distribution probability originates from other differences in initial conditions than those encapsulated in early-year WWV and cumulative WWE strength, which were very similar for both years. Other possibilities include the remote influence of SST anomalies external to the equatorial Pacific (Fig. 9, Zhu et al, 2016; Min et al, 2015) or the influence of remnants from the 2014 borderline weak El Niño (Levine and McPhaden, 2016; Hu and Fedorov, 2017) which left the equatorial pacific 0.5 to 1^{o}C warmer in early 2015 when compared to early 2014 (Fig. 1cd). Future studies will need to investigate the non-stochastic causes for the different forecasts distributions for these two years in order to isolate the associated sources of El Niño predictability.

References

Balmaseda MA, Mogensen K, Weaver AT (2013) Evaluation of the ecmwf ocean reanalysis system oras4. Quarterly Journal of the Royal Meteorological Society 139(674):1132–1161

Barnston AG, Tippett MK, L'Heureux ML, Li S, DeWitt DG (2012) Skill of Real-Time Seasonal ENSO Model Predictions during 2002–11: Is Our Capability Increasing? Bulletin of the American Meteorological Society 93(5):631–651, DOI 10.1175/BAMS-D-11-00111.1

Bellenger H, Guilyardi E, Leloup J, Lengaigne M, Vialard J (2014) ENSO representation in climate models: From CMIP3 to CMIP5. Climate Dynamics 42(7-8):1999–2018, DOI 10.1007/s00382-013-1783-z, arXiv:1011.1669v3

Bjerknes J (1966) A possible response of the atmospheric Hadley circulation to equatorial anomalies of ocean temperature. Tellus 18(4):820–829, DOI 10.3402/tellusa.v18i4.9712

Blanke B, Delecluse P (1993) Variability of the tropical atlantic ocean simulated by a general circulation model with two different mixed-layer physics. Journal of Physical Oceanography 23(7):1363–1388

Bougeault P (1985) A simple parameterization of the large-scale effects of cumulus convection. Monthly Weather Review 113(12):2108–2121

Boulanger JP, Durand E, Duvel JP, Menkes C, Delecluse P, Imbard M, Lengaigne M, Madec G, Masson S (2001) Role of non-linear oceanic processes in the response to westerly wind events: New implications for the 1997 El Niñoonset. Geophysical Research Letters 28(8):1603–1606, DOI 10.1029/2000GL012364

Boulanger JP, Menkes C, Lengaigne M (2004) Role of high- and low-frequency winds and wave reflection in the onset, growth and termination of the 1997-1998 El Niño. Climate Dynamics 22(2-3):267–280, DOI 10.1007/s00382-003-0383-8

Cai W, Borlace S, Lengaigne M, van Rensch P, Collins M, Vecchi G, Timmermann A, Santoso A, McPhaden MJ, Wu L, England MH, Wang G, Guilyardi E, Jin FF (2014) Increasing frequency of extreme El Niño events due to greenhouse warming. Nature Climate Change 5(2):1–6, DOI 10.1038/nclimate2100

Chang P, Zhang L, Saravanan R, Vimont DJ, Chiang JC, Ji L, Seidel H, Tippett MK (2007) Pacific meridional mode and el niño—southern oscillation. Geophysical Research Letters 34(16)

Chiodi AM, Harrison D (2015) Equatorial pacific easterly wind surges and the onset of la nina events. Journal of Climate 28(2):776–792

Eisenman I, Yu L, Tziperman E (2005) Westerly Wind Bursts: ENSO's Tail Rather than the Dog? Journal of Climate 18(24):5224–5238, DOI 10.1175/JCLI3588.1

Fedorov AV, Harper SL, Philander SG, Winter B, Wittenberg A (2003) How Predictable is El Niño? Bulletin of the American Meteorological Society 84(7):911–919, DOI 10.1175/BAMS-84-7-911

Fedorov AV, Hu S, Lengaigne M, Guilyardi E (2015) The impact of westerly wind bursts and ocean initial state on the development, and diversity of el niño events. Climate Dynamics 44(5-6):1381–1401

Gebbie G, Tziperman E (2009a) Incorporating a semi-stochastic model of ocean-modulated westerly wind bursts into an ENSO prediction model. Theoretical and Applied Climatology 97(1-2):65–73, DOI 10.1007/s00704-008-0069-6

Gebbie G, Tziperman E (2009b) Predictability of SST-modulated westerly wind bursts. Journal of Climate 22(14):3894–3909, DOI 10.1175/2009JCLI2516.1

Gebbie G, Eisenman I, Wittenberg AT, Tziperman E (2007) Modulation of Westerly Wind Bursts by Sea Surface Temperature: A Semistochastic Feedback for ENSO. Journal of the Atmospheric Sciences 64(9):3281–3295, DOI 10.1175/JAS4029.1

Guilyardi E (2006) El Niño - mean state - seasonal cycle interactions in a multi-model ensemble. Climate Dynamics 26:229–348

Guilyardi É, Madec G, Terray L (2001) The role of lateral ocean physics in the upper ocean thermal balance of a coupled ocean-atmosphere gcm. Climate Dynamics 17(8):589–599

Harrison DE, Vecchi GA (1997) Westerly wind events in the tropical pacific, 1986-95. Journal of Climate 10(12):3131–3156, DOI 10.1175/1520-0442(1997)010¡3131:WWEITT¿2.0.CO;2

Hewitt H, Copsey D, Culverwell I, Harris C, Hill R, Keen A, McLaren A, Hunke E (2011) Design and implementation of the infrastructure of hadgem3: The next-generation met office climate modelling system. Geoscientific Model Development 4(2):223–253

Hu S, Fedorov AV (2016) Exceptionally strong easterly wind burst stalling El Niño of 2014. Proceedings of the National Academy of Sciences 113(8):201514,182, DOI 10.1073/pnas.1514182113

Hu S, Fedorov AV (2017) The extreme el niño of 2015–2016: the role of westerly and easterly wind bursts, and preconditioning by the failed 2014 event. Climate Dynamics pp 1–19

Huang B, Banzon VF, Freeman E, Lawrimore J, Liu W, Peterson TC, Smith TM, Thorne PW, Woodruff SD, Zhang HM (2015) Extended reconstructed sea surface temperature version 4 (ersst. v4). part i: Upgrades and intercomparisons. Journal of climate 28(3):911–930

Jin FF (1997) An Equatorial Ocean Recharge Paradigm for ENSO. Part II: A Stripped-Down Coupled Model. DOI 10.1175/1520-0469(1997)054¡0830:AEORPF¿2.0.CO;2

Jin FF, Lin L, Timmermann A, Zhao J (2007) Ensemble-mean dynamics of the ENSO recharge oscillator under state-dependent stochastic forcing. Geophysical

Research Letters 34(3):L03,807, DOI 10.1029/2006GL027372
Kessler WS, McPhaden MJ, Weickmann KM (1995) Forcing of intraseasonal Kelvin waves in the equatorial Pacific. Journal of Geophysical Research 100(C6):10,613, DOI 10.1029/95JC00382
Kleeman R, Moore AM (1997) A theory for the limitation of enso predictability due to stochastic atmospheric transients. Journal of the atmospheric sciences 54(6):753–767
Kumar BP, Vialard J, Lengaigne M, Murty V, Mcphaden MJ, Cronin M, Pinsard F, Reddy KG (2013) Tropflux wind stresses over the tropical oceans: evaluation and comparison with other products. Climate dynamics 40(7-8):2049–2071
Larson SM, Kirtman BP (2015) An alternate approach to ensemble enso forecast spread: application to the 2014 forecast. Geophysical Research Letters 42(21):9411–9415
Le Moigne P, Boone A, Calvet J, Decharme B, Faroux S, Gibelin A, Lebeaupin C, Mahfouf J, Martin E, Masson V, et al (2009) Surfex scientific documentation. Note de centre (CNRM/GMME), Météo-France, Toulouse, France
Lengaigne M, Boulanger JP, Menkes C, Masson S, Madec G, Delecluse P (2002) Ocean response to the march 1997 westerly wind event. Journal of Geophysical Research: Oceans 107(C12)
Lengaigne M, Boulanger JP, Menkes C, Madec G, Delecluse P, Guilyardi E, Slingo J (2003) The March 1997 Westerly Wind Event and the onset of the 1997/98 El Niño: Understanding the role of the atmospheric response. Journal of Climate 16(20):3330–3343, DOI 10.1175/1520-0442(2003)016¡3330:TMWWEA¿2.0.CO;2
Lengaigne M, Boulanger JP, Menkes C, Delecluse P, Slingo J (2004a) Westerly Wind Events in the Tropical Pacific and their Influence on the Coupled Ocean-Atmosphere System: A Review. Earth's Climate: The Ocean-Atmosphere Interaction (January):49–69, DOI 10.1029/147GM03
Lengaigne M, Guilyardi E, Boulanger JP, Menkes C, Delecluse P, Inness P, Cole J, Slingo J (2004b) Triggering of El Niño by westerly wind events in a coupled general circulation model. Climate Dynamics 23(6):601–620, DOI 10.1007/s00382-004-0457-2
Lengaigne M, Menkes C, Aumont O, Gorgues T, Bopp L, André JM, Madec G (2007) Influence of the oceanic biology on the tropical pacific climate in a coupled general circulation model. Climate Dynamics 28(5):503–516
Levine AF, McPhaden MJ (2016) How the july 2014 easterly wind burst gave the 2015–2016 el niño a head start. Geophysical Research Letters 43(12):6503–6510
Lian T, Chen D, Tang Y, Wu Q (2014) Effects of westerly wind bursts on El Niño: A new perspective. Geophysical Research Letters 41(10):3522–3527, DOI 10.1002/2014GL059989
Lopez H, Kirtman BP (2014) Wwbs, enso predictability, the spring barrier and extreme events. Journal of Geophysical Research: Atmospheres 119(17)
Lorenz E (1993) The essence of chaosuniversity of washington press. Seattle, WA
Ludescher J, Gozolchiani A, Bogachev MI, Bunde A, Havlin S, Schellnhuber HJ (2014) Very early warning of next el niño. Proceedings of the national Academy of sciences 111(6):2064–2066
McPhaden M (2015) Playing hide and seek with el niño. Nature Climate Change
McPhaden MJ, Yu X (1999) Equatorial waves and the 1997–98 el nino. Geophysical Research Letters 26(19):2961–2964

McPhaden MJ, Zebiak SE, Glantz MH (2006a) ENSO as an integrating concept in earth science. Science (New York, NY) 314(5806):1740–1745, DOI 10.1126/science.1132588

McPhaden MJ, Zhang X, Hendon HH, Wheeler MC (2006b) Large scale dynamics and MJO forcing of ENSO variability. Geophysical Research Letters 33(16):L16,702, DOI 10.1029/2006GL026786

Meinen CS, McPhaden MJ (2000) Observations of Warm Water Volume Changes in the Equatorial Pacific and Their Relationship to El Nino and La Nina. Journal of Climate 13(20):3551–3559, DOI 10.1175/1520-0442(2000)013¡3551:OOWWVC¿2.0.CO;2

Menkes CE, Lengaigne M, Vialard J, Puy M, Marchesiello P, Cravatte S, Cambon G (2014) About the role of Westerly Wind Events in the possible development of an El Niño in 2014. Geophysical Research Letters 41(18):6476–6483, DOI 10.1002/2014GL061186

Min Q, Su J, Zhang R, Rong X (2015) What hindered the el niño pattern in 2014? Geophysical Research Letters 42(16):6762–6770

Molteni F, Buizza R, Palmer TN, Petroliagis T (1996) The ecmwf ensemble prediction system: Methodology and validation. Quarterly journal of the royal meteorological society 122(529):73–119

Molteni F, Stockdale T, Balmaseda MA, Balsamo G, Buizza R, Ferranti L, Magnusson L, Mogensen K, Palmer T, Vitart F (2011) The new ecmwf seasonal forecast system (system 4)

Paulson CA, Simpson JJ (1977) Irradiance measurements in the upper ocean. Journal of Physical Oceanography 7(6):952–956

Penland C, Sardeshmukh PD (1995) The Optimal Growth of Tropical Sea Surface Temperature Anomalies. Journal of Climate 8(8):1999–2024, DOI 10.1175/1520-0442(1995)008¡1999:TOGOTS¿2.0.CO;2

Puy M (2016) L'influence des coups de vent d'ouest dans le pacifique équatorial sur el niño: origines atmosphériques et impacts océaniques. PhD thesis, Paris 6

Puy M, Vialard J, Lengaigne M, Guilyardi E, Madec G (2015) Modulation of equatorial pacific wind events and their ocean response by atmospheric and oceanic large scale conditions Why are equatorial pacific wind events important to 1(July)

Puy M, Vialard J, Lengaigne M, Guilyardi E, Voldoire A, Madec G (2016) Modulation of equatorial pacific sea surface temperature response to westerly wind events by the oceanic background state. Climate Dynamics pp 1–25

Rayner N, Parker DE, Horton E, Folland C, Alexander L, Rowell D, Kent E, Kaplan A (2003) Global analyses of sea surface temperature, sea ice, and night marine air temperature since the late nineteenth century. Journal of Geophysical Research: Atmospheres 108(D14)

Reynolds RW, Rayner NA, Smith TM, Stokes DC, Wang W (2002) An improved in situ and satellite sst analysis for climate. Journal of climate 15(13):1609–1625

Roullet G, Madec G (2000) Salt conservation, free surface, and varying levels: a new formulation for ocean general circulation models. Journal of Geophysical Research: Oceans 105(C10):23,927–23,942

Seiki A, Takayabu YN (2007a) Westerly Wind Bursts and Their Relationship with Intraseasonal Variations and ENSO. Part II: Energetics over the Western and Central Pacific. Monthly Weather Review 135(10):3346–3361, DOI 10.1175/MWR3503.1

Seiki A, Takayabu YN (2007b) Westerly Wind Bursts and Their Relationship with Intraseasonal Variations and ENSO. Part II: Energetics over the Western and Central Pacific. Monthly Weather Review 135(10):3346–3361, DOI 10.1175/MWR3503.1

Smith R (1990) A scheme for predicting layer clouds and their water content in a general circulation model. Quarterly Journal of the Royal Meteorological Society 116(492):435–460

Stockdale TN, Anderson DL, Alves JOS, Balmaseda MA (1998) Global seasonal rainfall forecasts using a coupled ocean–atmosphere model. Nature 392(6674):370–373

Tollefson J (2014) El niño tests forecasters. Nature 508(7494):20

Valcke S, Caubel A, Declat D, Terray L (2003) Oasis3 ocean atmosphere sea ice soil user's guide. Prisim project report 2

Vecchi GA, Harrison D (2000) Tropical pacific sea surface temperature anomalies, el niño, and equatorial westerly wind events. Journal of climate 13(11):1814–1830

Vitart F, Alonso Balmaseda M, Ferranti L, Anderson D (2003) Westerly wind events and the 1997/98 el niño event in the ecmwf seasonal forecasting system: A case study. Journal of climate 16(19):3153–3170

Voldoire A, Sanchez-Gomez E, y Mélia DS, Decharme B, Cassou C, Sénési S, Valcke S, Beau I, Alias A, Chevallier M, et al (2013) The cnrm-cm5. 1 global climate model: description and basic evaluation. Climate Dynamics 40(9-10):2091–2121

Weisheimer A, Corti S, Palmer T, Vitart F (2014) Addressing model error through atmospheric stochastic physical parametrizations: impact on the coupled ecmwf seasonal forecasting system. Phil Trans R Soc A 372(2018):20130,290

Yu L, Rienecker MM (1999) Mechanisms for the indian ocean warming during the 1997–98 el nino. Geophysical Research Letters 26(6):735–738

Zhang T, Sun DZ (2014) Enso asymmetry in cmip5 models. Journal of Climate 27(11):4070–4093

Zhu J, Kumar A, Huang B, Balmaseda MA, Hu ZZ, Marx L, Kinter III JL (2016) The role of off-equatorial surface temperature anomalies in the 2014 el niño prediction. Scientific reports 6

Acknowledgements JV and ML acknowledge funding by Institut de Recherche pour le Développement (IRD). EG acknowledges funding by the Centre National de la Recherche Scientifique (CNRS) and from the National Centre for Atmospheric Science, a UK Natural Environment Research Council collaborative centre. This work was co-funded by a French Ministère de l'Education Nationale et de la Recherche grant, by a grant from the Agence Nationale de la Recherche MORDICUS, under the "Programme Environnement et Société" [Grant no. ANR-13-SENV-0002-02] and by the GOTHAM Belmont project (Grant no. ANR-15-JCLI-0004-01). This is PMEL contribution 4528.